# Fluid-Structure Interaction Simulation of Detonation-Driven Rupture Events of Thin-Walled Tubes with a Parallel Adaptive Level Set Method

Ralf Deiterding[a], Sean P. Mauch[a] and Fehmi Cirak[b]

[a]California Institute of Technology, Mail Code 158-79, Pasadena, CA 91125, USA

[b]University of Cambridge, Department of Engineering, Cambridge, CB2 1PZ, UK

Technically relevant fluid-structure interaction simulation of detonation-induced dynamic response of thin-walled solid structures requires an efficient detonation solver that can cope with large deformations as well as arbitrary topology changes of the computational domain. We present a parallel adaptive method that uses a scalar level set function to represent embedded evolving solid boundaries on an Eulerian Cartesian mesh and that employs a constant volume burn model for efficient detonation propagation in a shock-capturing finite volume scheme. As realistic computational application, we consider the induction of large plastic deformations and the fracture of thin aluminum tubes due to the passage of fully developed detonations in ethylene-oxygen mixtures.

## 1. INTRODUCTION

The Center for Simulation of Dynamic Response of Materials at the California Institute of Technology has recently completed the construction of an infrastructure for fluid-structure interaction (FSI) simulation involving compressible fluids named "Virtual Test Facility" (VTF) [1,2]. The approach targets highly instationary coupled problems, such as the rupture and fragmentation of solid structures under shock or detonation wave impact. In this regime, computational fluid dynamics (CFD) and computational solid dynamics (CSD) solver both need to be time-accurate and have to consider all arising supersonic wave phenomena correctly. Applicable numerical schemes are usually shock-capturing and time-explicit.

The design of the VTF follows a partitioned approach in which dynamically adaptive Cartesian CFD solvers can be invoked together with different CSD solvers. Fluid and solid are assumed to occupy disjoint parts of the computational domain and interaction is accomplished by exchanging boundary conditions only at the fluid-solid interface after consecutive time steps. For compressible fluids, stable solutions are obtained reliably with such a "weakly coupled" method, when the evolving interface geometry and velocities are imposed as boundary conditions on the CFD solver and the hydrodynamic pressure is used as force boundary condition acting on the solid exterior [3,4].

In the present paper, we apply the VTF to simulating rupture events of thin-walled aluminum tubes due to the passage of gaseous detonations in ethylene-oxygen mixtures [5]. Emphasis is put on the description of the components on the CFD side that have

proven crucial for these computations: a dynamically adaptive Cartesian upwind scheme with embedded thin-structure capability and a constant volume combustion model for resolution-independent detonation propagation, cf. Sec. 2. Specific to the VTF is that scalar level set functions storing the distance information to the embedded surface are used to represent the complex geometry on the Cartesian fluid mesh and a ghost-fluid-type approach is employed to impose fluid boundary conditions [6]. In Sec. 3, we outline the auxiliary algorithm based on geometric characteristic reconstruction and scan conversion that we have developed to transform evolving triangulated surface meshes efficiently into signed or unsigned distance functions. After the validation of the detonation model in Sec. 4, we present in Sec. 5 two FSI computations with a Lagrangian thin-shell CSD solver [7]. The first simulation verifies our methodology for detonation-driven large plastic deformations; the second computation is a preliminary result for the fracturing case.

## 2. EULERIAN DETONATION SOLVER

The governing equations of detonation wave propagation in gases are the inviscid Euler equations [9]. Throughout this paper, we consider only the simplified case of a single exothermic chemical reaction $A \longrightarrow B$ with a progress variable $Y$ corresponding to the mass fraction ratio between the partial density of the reactant $A$ and the total density $\rho$, i.e. $Y = \rho_A/\rho$. The governing equations of the hydrodynamic model are

$$\begin{array}{rcl rcl} \partial_t\rho + & \nabla\cdot(\rho\vec{u}) & = 0\,, & \partial_t(\rho\vec{u}) + & \nabla\cdot(\rho\vec{u}\otimes\vec{u}) + \nabla p & = 0\,, \\ \partial_t(\rho E) + & \nabla\cdot((\rho E + p)\vec{u}) & = 0\,, & \partial_t(Y\rho) + & \nabla\cdot(Y\rho\vec{u}) & = \psi\,. \end{array} \tag{1}$$

Herein, $\vec{u}$ is the velocity vector and $E$ the specific total energy. The hydrostatic pressure $p$ is given by $p = (\gamma-1)(\rho E - \frac{1}{2}\rho\vec{u}^T\vec{u} - \rho Y q)$ with $\gamma$ denoting the ratio of specific heats and $q$ the heat release due to the chemical reaction per unit mass. A one-step reaction would typically be modeled with an Arrhenius law such as [9]

$$\psi = -kY\rho\exp\left(\frac{-E_A\rho}{p}\right), \tag{2}$$

but in the specific case considered here, we utilize the constant volume burn model suggested by Mader [8]. This model neglects the detailed chemical depletion, and therefore the internal detonation structure, but ensures correct speed of propagation and state in chemical equilibrium at all grid resolutions. The model is intended to be applied together with the fractional step method that numerically decouples chemical reaction and hydrodynamic transport. First, the *homogeneous* system (1) is advanced at a full time step, then the reactant density $\rho_A$, pressure $p$, and total energy $E$ are modified locally in each finite volume cell; the total density $\rho$ and the velocity vector $\vec{u}$ remain unaltered. The algorithm for the detonation model reads:

$V := \rho^{-1}$, $V_0 := \rho_0^{-1}$, $V_{CJ} := \rho_{CJ}$
$Y' := 1 - (V - V_0)/(V_{CJ} - V_0)$
if $0 \le Y' \le 1$ and $Y > 10^{-8}$
  if $Y < Y'$ and $Y' < 0.9$ then $Y' := 0$
  if $Y' < 0.99$ then $p' := (1-Y')p_{CJ}$ else $p' := p$
  $\rho_A := Y'\rho$, $E := p'/(\rho(\gamma-1)) + Y'q_0 + \frac{1}{2}\vec{u}^T\vec{u}$

In the latter, the index 0 indicates the unreacted state (assumed to be constant), while CJ refers to the equilibrium values that can be calculated in advance following Chapman-Jouguet theory [9,10] for a given detonation velocity.

As shock-capturing finite volume upwind scheme, we utilize a straightforward extension of the flux-vector splitting method by Van Leer, cf. [10]. Second-order accuracy in smooth solution regions is achieved with the MUSCL-Hancock variable extrapolation technique. Geometrically complex moving boundaries are incorporated into the upwind scheme by using some of the finite volume cells as ghost cells for enforcing immersed moving wall boundary conditions [6,11]. The boundary geometry is mapped onto the Cartesian mesh by employing a scalar level set function $\phi$ that stores the unsigned distance to the boundary surface and allows the efficient evaluation of the boundary outer normal in every mesh point as $\vec{n} = -\nabla\phi/|\nabla\phi|$.[1] A cell is considered to be a valid fluid cell, if the distance at the cell *midpoint* satisfies the condition $\phi > h/2$ and as an exterior ghost cell otherwise. The mesh received from a thin-shell solver corresponds to a two-dimensional manifold surface mesh and the utilization of condition $\phi > h/2$ is a straightforward, unambiguous solution to achieve the mandatory thickening of this mesh by the shell thickness $h$. The contour line $\phi = h/2$ effectively represents the embedded boundary for the fluid solver (depicted as dotted line around shell elements in Fig. 1). The hydrodynamic load on each shell element is evaluated as the difference between the approximated pressure values at $\phi = h/2$ in the positive and negative direction of each shell element's normal, i.e. $p^F := p^+ - p^-$.

The value construction in the cells used to prescribe boundary conditions along embedded moving rigid walls has been detailed in [12]. It involves a monotonicity-preserving mirroring of spatially interpolated values across the boundary, which we accomplish by a combination of linear interpolation and one-sided constant value extrapolation. Figure 1 visualizes the interpolation stencil reduction near the boundary for three exemplary cases. After each fluid time step, internal ghost cells are set to the values of the nearest interior cell to ensure proper values in case of boundary movement. Note that a ghost-cell-based technique does not require a modification of the numerical stencil itself and is therefore generically applicable, but causes a diffusion of the boundary location throughout the method and results in an overall non-conservative scheme. We alleviate such errors and the unavoidable staircase approximation of the boundary with this approach effectively by using isotropic dynamic mesh adaptation to refine the Cartesian mesh along the boundary.

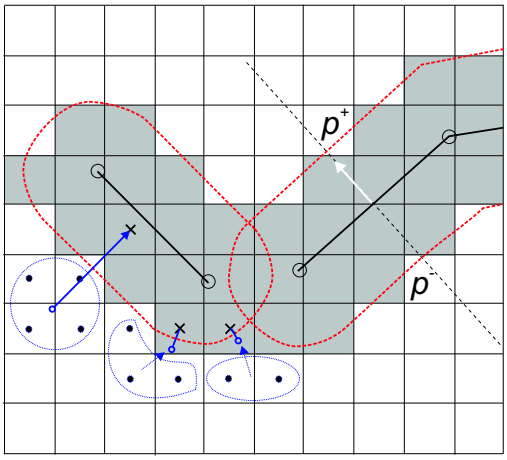


Figure 1: Ghost cells (shaded gray) around 1d shell elements (black lines) and construction of mirrored values.

Cartesian fluid mesh adaptation in the VTF is generically provided by the structured adaptive mesh refinement (SAMR) framework AMROC [14]. AMROC (Adaptive Mesh Refinement in Object-oriented C++) implements the SAMR method after Berger and Colella [13] that combines temporal with spatial resolution adaptation

[1] For topologically closed boundary surfaces it is also possible to use signed distance instead, cf. [12,7].

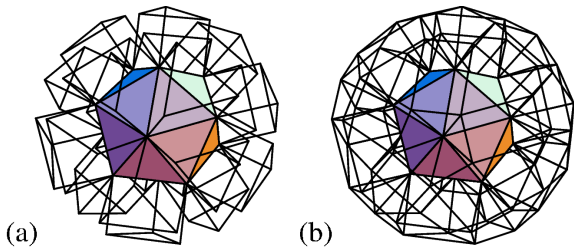


Figure 2. The characteristic polyhedra for faces and edges of an icosahedron.

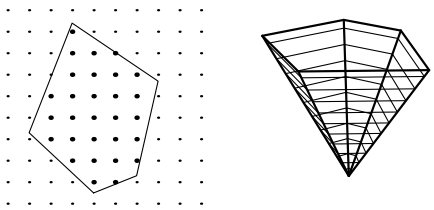

Figure 3. Slicing of a polyhedron to form two-dimensional polygons (right) and scan conversion of an exemplary case (left).

and has been tailored for time-explicit finite volume schemes. Our extension of the recursive Berger-Collela SAMR algorithm for weakly coupled FSI simulation has been described in detail in [12]. The parallelization strategy in AMROC is a locality-preserving rigorous domain decomposition approach that employs a space-filling curve for dynamic run time partitioning. A representative scalability study is also discussed in [12].

## 3. EFFICIENT LEVEL SET EVALUATION

The CFD method described in the previous section is based on the concept of employing a distance function to represent a complex embedded boundary on a Cartesian mesh implicitly. While distance functions are easily prescribed for single elementary geometric objects, their evaluation can be very cumbersome for complex shapes. In coupled FSI simulations, this complex shape is defined by the deforming surface mesh provided by a CSD solver. Up to now, all CSD solvers in the VTF are unstructured Lagrangian finite element solvers that export a triangular interface mesh.

One can efficiently compute the distance on a grid by solving the Eikonal equation with the method of characteristics and utilizing polyhedron scan conversion [15]. For a given grid point, the relevant closest point on the triangular mesh lies on one of the primitives (faces, edges and vertices) that comprise the surface. The characteristics emanating from each of these primitives form polyhedral shapes. Such a *characteristic polyhedron* contains all of the points which are possibly closest to its corresponding face, edge or vertex. The closest points to a triangle face must lie within a triangular prism defined by the face and its normal; the closest points to an edge lie in a cylindrical wedge defined by the line segment and the normals to the two incident faces (see Fig. 2 for face (a) and edge (b) polyhedra for a particular example). Analogously, polygonal pyramids emanating from the vertices are also possible (not shown). We then determine the grid points that lie inside a characteristic polyhedron with polyhedron scan conversion. The polyhedron is sliced along each sheet of the grid lattice to produce two-dimensional polygons. Rasterization is then used to determine which Cartesian points lie inside a particular polygon, cf. Fig. 3. Simple geometric formulas are finally applied to evaluate the distance between each grid point and the mesh primitive found to be closest. By evaluating the distance exactly only within a small band around the embedded surface, a highly efficient transformation algorithm can be formulated. It has linear computational complexity both in the number of Cartesian mesh points and surface triangles [15,1].

## 4. DETONATION SOLVER VERIFICATION

The configuration we are interested in is an experimental setup developed by Chao [5]. It consists of a detonation tube of 1.52 m length to which thin-walled aluminum (Al6061-T6) test tubes are attached. The test specimen have a length from 45.7 cm to 89.6 cm, an inner radius of 1.975 cm, and a wall thickness of 0.89 mm. While the lower end of the device is closed, a thin diaphragm seals the upper end. The entire apparatus is filled with a perfectly stirred mixture of stoichiometric ethylene and oxygen ($C_2H_4 + 3\,O_2$) at 295 K. Combustion is thermally ignited at the closed end and accelerates quickly to a quasi-stationary detonation wave. A Taylor rarefaction wave occurs immediately behind the detonation and must be considered in accurate simulations. All computations use a constant adiabatic mixture coefficient of $\gamma = 1.24$.

In order to ensure the correct function of the detonation model sketched in Sec. 2, we carry out one-dimensional simulations for an initial pressure of $p_0 = 100\,\text{kPa}$. The heat release is set to $q = 4.704\,\text{MJ/kg}$ leading to a detonation velocity of 2291.74 m/s. This average speed of propagation has been measured in experiments for this particular configuration [5]. We use a one-dimensional setup with a domain length of 2.15 m encompassing the detonation tube and the longest specimen, reflective wall boundary conditions at the lower end and zero gradient outflow conditions at the upper domain boundary. A mesh of 1148 cells plus one additional level of cells all refined by a factor 4 is used. The adaptation criteria are scaled gradients of total density, pressure and mass fraction $Y$. Figure 4 gives a comparison of the temporal pressure traces at the locations $x = 0.38\,\text{m}$ (transducer 1), $x = 0.78\,\text{m}$, and $x = 1.18\,\text{m}$ (from left to right in Fig. 4) in the one-dimensional simulation with experimentally measured pressure traces (time origins in both traces adjusted to $t = 0$ when the detonation front reaches transducer 1). The agreement is very good considering the natural fluctuations in experimental measurements and the idealized ignition in our inviscid model.

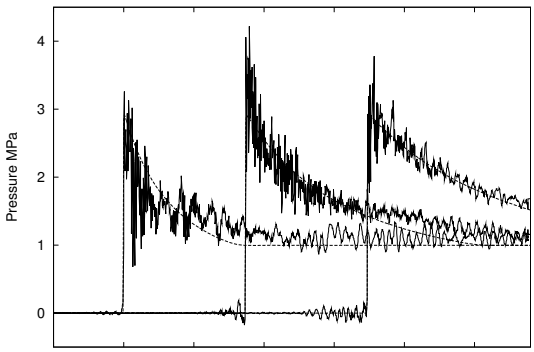


Figure 4: Comparison of measured (solid) and simulated (dashed) pressure traces.

## 5. FLUID-STRUCTURE INTERACTION SIMULATIONS

In three space-dimensions, we ensure the correct consideration of the Taylor rarefaction wave, cf. Fig. 4, by considering an additional tubular domain 0.92 m upstream in the CFD solver. The flow field is initialized with the data from corresponding one-dimensional simulations taken at the moment when the detonation enters the specimen. The dynamic material response of the test specimen itself is computed with a Lagrangian CSD solver following Kirchhoff-Love-type thin-shell theory [7]. The solver uses sub-division finite elements [16] as a robust discretization approach for shells and special interface elements to model material rupture [17]. The fluid-structure coupling methodology is a straightforward partitioned approach in which CFD and CSD solver are parallelized separately using independent rigorous domain decomposition methods. Exchange of inter-solver bound-

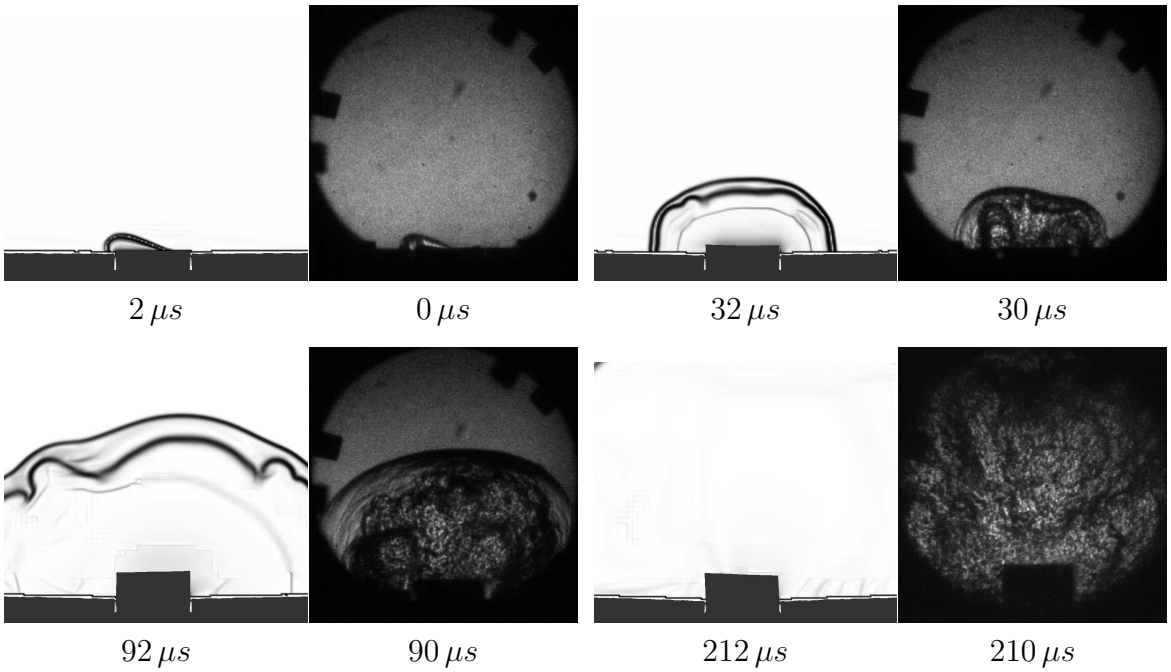


Figure 5. Simulated schlieren pictures of fluid density and side view of the deforming solid mesh compared to schlieren photo graphs taken in a corresponding experiment.

ary conditions along the distributed fluid-shell boundary is facilitated through a special non-blocking communication library. The computations employ the FSI communication algorithm detailed in [12] that considers the recursive time step refinement in the SAMR CFD solver and allows additionally for sub-iterations in the CSD solver accommodating a typically smaller solid time step.

As a verification test towards rupture that involves large plastic material deformations, an experiment has been conducted in which an "H" shape pattern is cut close to the middle into a specimen of 89.6 cm. Each cut has a length of 25 mm. The combustible mixture is the same as in Sec. 4. When the detonation wave passes the pre-flawed region, the two flaps open up and the high pressure in the Taylor wave causes a venting of the combustion products into the air. To allow for an undisturbed leakage we use a relative large computational domain of $[-92\,\text{cm}, 89.6\,\text{cm}] \times [-3.75\,\text{cm}, 56.25\,\text{cm}] \times [-39\,\text{cm}, 39\,\text{cm}]$ and an SAMR base mesh of $104 \times 80 \times 242$ cells with 3 additional level and refinement factors 2, 2, and 4. Additional to the refinement criteria in Sec. 4, that capture the detonation front, the walls of the specimen are always fully refined enabling an offset parameter of $h = 0.81\,\text{mm}$. An exemplary snapshot of the evolving mesh is depicted in Fig. 6. The figure shows schlieren of the fluid density on the three refinement levels displayed in different gray tones and highlights the enormous gain from dynamic mesh adaptation. An equivalent unigrid CFD calculation would require $> 7.9 \cdot 10^9$ cells, but the SAMR computation uses only $\approx 4.0 \cdot 10^7$ cells on average. The CSD sub-

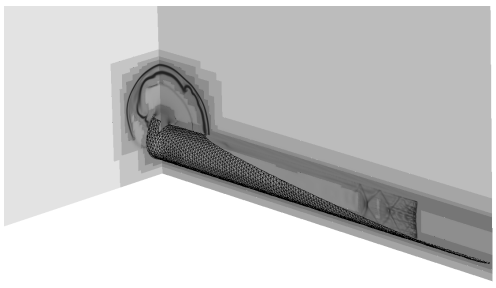

Figure 6: Fluid mesh adaptation and deforming solid mesh at $92\,\mu s$.

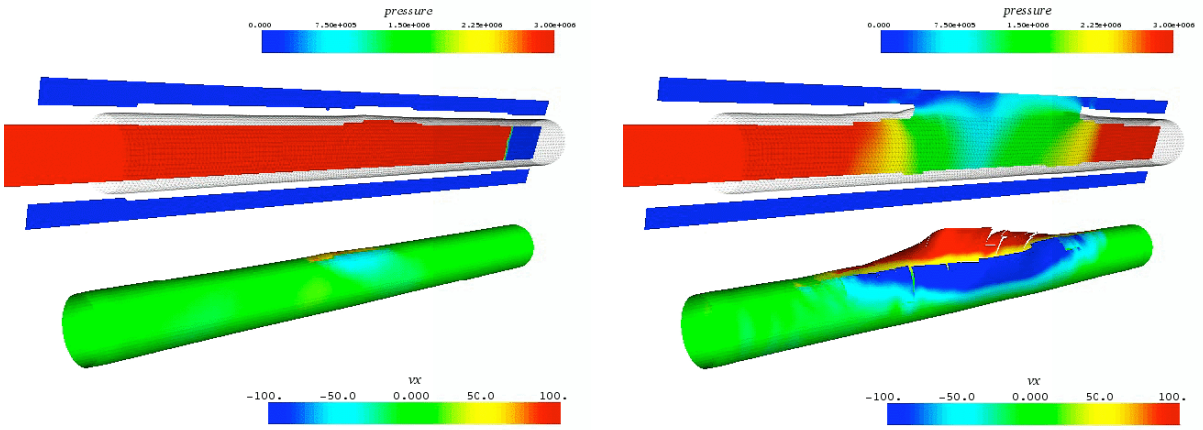


Figure 7. Detonation-driven rupture of the thin aluminum tube. Snapshots of the solid mesh with velocity iso-contours (lower row) and cuts through the fluid domain show the opening due to fracture and the resulting hydrodynamic venting (upper row).

problem employs a triangular input mesh of 17,056 elements. A J2 plasticity model for aluminum with power-law hardening and thermal softening is applied as bulk material model [18].

The computation ran on 72 Opteron-2.2 GHz processors connected with Infiniband network for about 4300 h CPU to a final time of $t_e = 460\,\mu$s. In Fig 5, a series of schlieren photo graphs are compared to corresponding simulated images at a nearby time. The computational graphics display schlieren of the fluid density in the plane perpendicular to the z-axis together with a side view of the deforming solid mesh. The time origin is set to the moment when the detonation passes the middle of the longitudinal slot. The agreement in flow evolution and solid deformation is quite good confirming the correct function of the fluid-structure coupling methodology and the appropriateness of the chosen computational setup.

Finally, we present one exemplary fluid-structure interaction computation that involves the rupture of the test specimen utilizing the fracture capability of the thin-shell CSD solver [17]. The initial pressure is $p_0 = 180\,$kPa and the specimen has a length of 45.7 cm. To ensure a reproducible fracture the specimen has a central longitudinal notch of 6.32 cm at the middle, which is modeled as an initial crack in the computations. Figure 7 visualizes the results for a shell mesh of 8665 elements and a uniform Cartesian fluid mesh of $40 \times 40 \times 725$ cells that required $\approx 900\,$h CPU on 27 nodes of a Pentium-4-2.4 GHz dual processor system (21 fluid and 33 solid processes). 1300 coupled time steps with fixed step size to a final time of $t_e = 260\,\mu$s have been calculated (20 solid solver sub-steps in each fluid time step). The left graphic of Fig. 7 shows the beginning of the crack opening $\approx 150\,\mu$s after the detonation has passed the initial crack. The snapshot on the right shows the rupture at the final time $260\,\mu$s. The venting of high pressurized reacted gas from the opening slit and the cracking of the material are clearly visible. It is worth pointing out that during this simulation, the dynamic level set evaluation with the algorithm sketched in Sec. 3 and the update with the core Cartesian finite volume scheme described in Sec. 2 have about the same computational costs on each fluid processor. This result confirms that our approach utilizing distance functions for implicit geometry

representation is sufficiently efficient for computing even complex FSI problems with large deformations and evolutions in the mesh topology with high computational efficiency.

## 6. CONCLUSIONS

A level-set-based Cartesian CFD solver tailored for time-accurate fluid-structure interaction simulation involving gaseous detonation waves and thin embedded solid structures has been described. The approach has been demonstrated to handle arbitrary topology changes and large deformations in reasonable agreement with experimental results. As enabling components for high computational efficiency we have detailed the employed detonation model and an effective distance function evaluation algorithm. The integrated implementation of these components together with the thin-shell CSD solver used throughout this paper in the software framework Virtual Test Facility is freely available for research purposes, see http://www.cacr.caltech.edu/asc.

## ACKNOWLEDGEMENTS

The authors would like to thank J. C. Krok, Z. Lianz, J. Karnesky, F. Pintgen, and J. E. Shepherd for providing the experimental results shown in the Figs. 4 and 5.

## REFERENCES

1. R. Deiterding, R. Radovitzky, et al., Engineering with Computers (2006), in press.
2. R. Deiterding, F. Cirak, S. Mauch, D.Meiron, Lec. Notes Comp. Sci. 3392 (2006) 122.
3. U. Specht, Numerische Simulation mechanischer Wellen an Fluid-Festkörper-Mediengrenzen, VDI Verlag, Düsseldorf, 2000.
4. R. Löhner, J. Baum, C. Charman, D.Pelessone, Lec. Notes Comp. Sci. 2565 (2003) 3.
5. T.-W. Chao, Gaseous detonation-driven fracture of tubes, PhD thesis, California Institute of Technology, 2004.
6. M. Arienti, P. Hung, E. Morano, J. Shepherd, J. Comput. Phys. 185 (2003) 213.
7. F. Cirak and R. Radovitzky, Computers & Structures, 83 (2005) 491.
8. C. L. Mader, Numerical modeling of detonations, Univ. Cal. Press, Berkeley, 1979.
9. W. Fickett, W. C. Davis, Detonation, Univ. Cal. Press, Berkeley, 1979.
10. R. Deiterding, Parallel adaptive simulation of multi-dimensional detonation structures, PhD thesis, Brandenburgische Technische Universität Cottbus, 2003.
11. R. P. Fedkiw, T. Aslam, B. Merriman, S. Osher, J. Comput. Phys. 152 (1999) 457.
12. R. Deiterding, Proc. Parallel CFD 2005, Elsevier, (2006), in press.
13. M. Berger and P. Colella, J. Comput. Phys. 82 (1988) 64.
14. R. Deiterding. AMROC - Blockstructured Adaptive Mesh Refinement in Object-oriented C++, http://amroc.sourceforge.net.
15. S. P. Mauch, Efficient Algorithms for Solving Static Hamilton-Jacobi Equations, PhD thesis, California Institute of Technology, 2003.
16. F. Cirak and M. Ortiz, Int. J. Numer. Meth. Engineering, 51 (2001) 813.
17. F. Cirak, M. Ortiz, A. Pandolfi, Computer Methods in Appl. Mechanics and Engineering, 194 (2005) 2604.
18. A. Cuitino and M. Ortiz, Engineering Computations 9 (1992) 437.